

Simulation of spiral instabilities in wide-gap spherical Couette flow

Suhail Abbas^{1,2}, Li Yuan^{1,2,4} and Abdullah Shah³

¹LSEC & Institute of Computational Mathematics and Scientific/Engineering Computing, Academy of Mathematics and Systems Science, Chinese Academy of Sciences, Beijing 100190, People's Republic of China

²School of Mathematical Sciences, University of Chinese Academy of Sciences, Beijing 100190, People's Republic of China

³Department of Mathematics, COMSATS Institute of Information Technology, Islamabad, Pakistan

E-mail: suhailkiu156@gmail.com, lyuan@lsec.cc.ac.cn and abdullah_shah@comsats.edu.pk

Received 11 May 2017, revised 15 November 2017

Accepted for publication 27 November 2017

Published 29 January 2018



CrossMark

Communicated by Edgar Knobloch

Abstract

We numerically study the wide-gap spherical Couette flow between two concentric spheres with the inner sphere rotating and the outer one stationary. Two wide-gap clearance ratios, $\beta = (R_2 - R_1)/R_1 = 0.33$ and 0.50 , are chosen to investigate the transition scenarios of the spiral instabilities with increasing Reynolds number (Re). For $\beta = 0.33$, we first obtain the steady 1-vortex flow at $Re = 700$ by using the 1-vortex flow for a medium gap $\beta = 0.18$ at $Re = 700$ as the initial condition. The 1-vortex flow for $\beta = 0.33$ exists for $Re \in [450, 2050]$ and it collapses back to the basic flow when $Re > 2050$. We then detect spiral instabilities by increasing the Reynolds number gradually. The basic flow becomes unstable at $Re_{c1} = 2900$ where spiral waves of wavenumber $m = 6$ appear first. Increasing the Reynolds number further, the wavenumber decreases to 5 and 4 at $Re_{c2} = 3000$ and $Re_{c3} = 4000$ respectively. The flow becomes turbulent when $Re > 4500$. For $\beta = 0.50$, no Taylor vortices are found. The basic flow becomes unstable at $Re_{c1} = 1280$ where spiral waves of wavenumber $m = 5$ occur first. As the Reynolds number is increased, the wavenumber becomes 4 at $Re_{c2} = 1700$, 5 again at $Re_{c3} = 1800$, 4 at $Re_{c4} = 2000$, and becomes 3 at $Re_{c5} = 2200$ while the flow becomes turbulent for $Re > 2200$. The computed rotational frequencies as a function of the Reynolds number for

⁴ Author to whom any correspondence should be addressed.

spiral waves of wavenumber $m = 5, 4$ and 3 are in good agreement with previous experimental results. The present transition scenario of the spiral wavenumber with increasing Reynolds number for $\beta = 0.33$ is the same as that of Egbers and Rath (1995 *Acta Mech.* **111** 125–40), while for $\beta = 0.50$, it is only partially similar to those of Wulf *et al* (1999 *Phys. Fluids* **11** 1359–72) and Egbers and Rath (1995 *Acta Mech.* **111** 125–40).

Keywords: spherical Couette flow, wide gap, Taylor vortex, spiral wave

(Some figures may appear in colour only in the online journal)

1. Introduction

In this paper, we study the spiral instabilities in the laminar-turbulent transition in the wide-gap spherical Couette flow (SCF) between two concentric spheres. The rotation of fluid in a spherical shell (the spherical Couette system) is relevant to astrophysical and geophysical processes (Wimmer 1988, Sha and Nakabayashi 2001). In this study, we assume that the inner sphere is rotating and the outer one is fixed while the spherical gap is filled with a Newtonian fluid. The flow has only two control parameters: a Reynolds number $Re = \Omega R_1^2 / \nu$, and a clearance ratio (gap width) $\beta = (R_2 - R_1) / R_1$, where Ω is the angular velocity of the inner sphere, ν is the kinematic viscosity of the fluid, and R_1, R_2 are the radii of the inner and outer spheres respectively. It is well-known that besides the two control parameters, the flow history such as rotational acceleration of the inner sphere, initial flowfield and wave form of perturbation added may also play a role in the formation of different types of supercritical disturbances (e.g., different Taylor–Görtler (TG) vortices, spiral waves, ring vortices, Stuart waves, etc). Owing to the simple geometry and the diversity of instabilities, SCF is an ideal template for studying symmetry-breaking bifurcations during the laminar-turbulent transition.

Most of the previous numerical and experimental investigations on SCF were carried out for narrow and medium gap widths (Sawatzki and Zierep 1970, Munson and Menguturk 1975, Wimmer 1976, Yavorskaya *et al* 1980, Bartels 1982, Nakabayashi 1983, Schrauf 1986, Marcus and Tuckerman 1987a, 1987b, Bühler and Zierep 1987, Nakabayashi and Tsuchida 1995, Yuan *et al* 1996, Yuan 2004, 2012, etc). For narrow and medium gap widths, the first instability occurs in the form of toroidal TG vortices, while for wide gap widths, the first instability occurs in the form of spiral vortices or spiral waves (Dumas 1991, Dumas and Leonard 1994, Egbers and Rath 1995, Zikanov 1996, Araki *et al* 1997, Wulf *et al* 1999, Sha and Nakabayashi 2001, Hollerbach *et al* 2006). Most of the investigators divided the clearance ratio into narrow-, medium- and wide-gap regions while Nakabayashi *et al* (2002) divided the clearance ratio into four regions. In his classification, the narrow-gap region refers to $0 < \beta < \beta_N \approx 0.13$ for which cylinder-type disturbances such as spiral TG vortices and traveling waves play an important role. The intermediate-gap region defined by him is $\beta_N < \beta < \beta_I \approx 0.17$ for which the spiral TG vortices and the traveling waves occurring as a result of the second instability (Höpf bifurcation) disappear with increasing Reynolds number. The medium-gap region refers to $\beta_I < \beta < \beta_W \approx 0.3$ for which neither spiral TG vortices nor traveling waves on TG vortices occur. Instead, disk-type disturbances such as Stuart vortices and shear waves occur in the high latitude zones along with TG vortices near the equator at high Reynolds number. The wide-gap region refers to $\beta > \beta_W$ for which the non-axisymmetric instability (spiral vortices or spiral waves) instead of the Taylor instability occurs as the first instability. We note that some calculations (Schrauf 1986, Hollerbach 1998, Loukopoulos and Karahalios 2004) obtained TG

vortices for the range of $0.24 \leq \beta \leq 0.4963$ (medium to wide gaps) by using special initial conditions, while some experiments claimed that no TG vortices for $\beta > 0.3$ (Nakabayashi *et al* 2002) or $\beta > 0.4$ (Yavorskaya *et al* 1980) exist.

Many researchers studied flow instabilities and transition to turbulence in wide-gap SCF. Munson and Menguturk (1975) carried out the first experimental study and reported flow instability at $Re = 407$ for $\beta = 1.27$ and $Re = 425$ for $\beta = 2.29$. Belyaev *et al* (1978) and Belyaev and Yavorskaya (1991) considered $\beta = 1.33, 1.0$ and 0.54 to obtain spiral waves of wavenumber $m = 3, 4, 5$ at critical Reynolds numbers 406, 463 and 1120 respectively.

Subsequent more detailed experimental studies on wide-gap SCF were carried in 1990s (Egbers and Rath 1995, Wulf *et al* 1999). Egbers and Rath (1995) considered $\beta = 0.33$ and 0.50 . For $\beta = 0.50$, they obtained secondary spiral waves with an azimuthal wavenumber $m = 5$ at $Re_{c1} = 1244$, and with increasing Re number, the wavenumber decreases monotonically. They have shown $m = 4$ at $Re = 1583$, $m = 3$ at $Re = 1810$ while the flow becomes turbulent for higher Reynolds numbers. Wulf *et al* (1999) provided more clear flow visualizations for the same two clearance ratios. For $\beta = 0.50$, Wulf *et al* (1999) obtained spiral waves of wavenumber $m = 5$ at $Re_{c1} = 1190$, $m = 4$ at $Re_{c2} = 1395$ and $m = 3$ at $Re_{c3} = 1565$ while the transition scenario with further increasing Reynolds number was different from that of Egbers and Rath (1995). Specifically, they obtained traveling spiral waves of wavenumber $m = 5$ again at $Re_{c4} = 1710$ and aperiodic traveling spiral waves of $m = 4$ at $Re_{c5} = 2080$ while the flow becomes turbulent for $Re > Re_{c6} \approx 2380$.

For $\beta = 0.33$, Egbers and Rath (1995) obtained spiral waves of wavenumber $m = 6$ at $Re_{c1} = 2628$, then obtained wavenumber $m = 5$ and 4 at $Re = 2800$ and 3100 respectively. By further increasing Re number, the flow becomes turbulent. However, Wulf *et al* (1999) reported a very different scenario. First they obtained a spiral vortex with its center at the pole for a critical Reynolds number $Re_{c1} = 2395$, which evolves into a ring vortex at $Re_{c2} = 2815$, and then spiral waves of wavenumber $m = 6$ appear at $Re_{c3} = 3300$. Increasing the Reynolds number still further, three of the six spiral waves become weak, and aperiodic coherent structures appear at $Re_{c4} = 3385$, and finally the flow becomes turbulent at $Re \geq 3800$.

Numerical studies on wide-gap SCF were initiated by Dumas (1991) and Dumas and Leonard (1994). Dumas (1991) simulated $\beta = 1.27, 1.0$ and 0.54 . He obtained spiral waves of wavenumber $m = 3$ for $\beta = 1.27$ at $Re_c = 406$ having good agreement with the experimental value $Re_c = 407$ (Munson and Menguturk 1975). They also found critical Reynolds numbers $Re_c = 489$ and 1122 for $\beta = 1.0$ and 0.54 respectively which are very close to 463 and 1120 of Belyaev *et al* (1978). Later, Araki *et al* (1997) computed the flow for $\beta = 0.50$, and obtained spiral waves of wavenumber $m = 5$ at $Re_c = 1245$, which is very close to the experimental value of 1244 in Egbers and Rath (1995). Hollerbach (2000) computed the flow for a different $\beta = 0.34$ and obtained spiral waves of wavenumber $m = 6$ at $Re_c = 2684$. Later, Hollerbach *et al* (2006) carried out another numerical study on wide-gap SCF. They considered $0.1 \leq \beta \leq 3.8$, and showed that the wavenumber decreases monotonically from $m = 12$ at $\beta = 0.1$ to $m = 2$ at $\beta = 3.8$.

As discrepancies existed in the literature, particularly for $\beta = 0.33$ and 0.50 , for which Egbers and Rath (1995) and Wulf *et al* (1999) presented different transition scenarios, it is necessary to further examine the evolution of spiral instabilities with increasing Reynolds number for the two clearance ratios. In this work, we have carried out time-dependent simulations for the two clearance ratios by solving the 3D unsteady incompressible Navier–Stokes equations numerically with a finite difference method.

For $\beta = 0.33$, our simulation gives the evolution scenario of the spiral waves with increasing Reynolds number: $m = 6 \rightarrow 5 \rightarrow 4 \rightarrow$ turbulent flow, which agrees with

that of Egbers and Rath (1995). For $\beta = 0.50$, our evolution scenario is $m = 5 \rightarrow 4 \rightarrow 5 \rightarrow 4 \rightarrow 3 \rightarrow$ turbulent flow, which partially follows the experimental result of Wulf *et al* (1999): $m = 5 \rightarrow 4 \rightarrow 3 \rightarrow 5 \rightarrow 4 \rightarrow$ turbulent flow, and partially follows that of Egbers and Rath (1995): $m = 5 \rightarrow 4 \rightarrow 3 \rightarrow$ turbulent flow. Nevertheless, the calculated rotational frequencies and wavenumber of the spiral waves at several Reynolds numbers for the two clearance ratios are in approximate agreement with Egbers and Rath (1995) and Wulf *et al* (1999).

In section 2, we briefly describe the computational setup. Section 3 deals with numerical results and discussion of the characteristics of the wide-gap instabilities in the form of spiral waves of different wavenumber and wave frequencies. Section 4 concludes this paper.

2. Computational setup

Consider an annulus between two concentric spheres filled with an incompressible Newtonian fluid of constant density ρ and kinematic viscosity ν . The inner sphere rotates with an angular velocity Ω , while the outer sphere is fixed. For simulating the incompressible flow we have used the artificial compressibility method discretized with a finite difference weighted non-oscillatory (WENO) scheme (Yang *et al* 1998, Jiang and Wu 1999) and solved with a line Gauss–Seidel method (Rogers and Kwak 1990, Yuan 2002).

We divide the spherical annulus into a number of grid points along the radial (r), meridional (θ) and azimuthal (ϕ) directions, respectively. The grid points are clustered near the walls along the radial (r) direction and uniform along the meridional (θ) and azimuthal (ϕ) directions. Wider gaps need more grid points in the radial direction. We use grid point numbers $51(r) \times 361(\theta) \times 153(\phi)$ for $\beta = 0.33$ and $61(r) \times 361(\theta) \times 153(\phi)$ for $\beta = 0.50$. The non-dimensional physical time step $\Delta t = 0.05$ is used. The Stokes flow (Marcus and Tuckerman 1987a) is used as an initial condition.

We apply no-slip boundary conditions to the velocities on the inner and outer spheres. The pressure on the wall is obtained from the radial component of the momentum equations written in the spherical coordinate system, and the polar boundary is treated by a half grid size arrangement as in Yuan (2002). We take a reference pressure at a fixed interior point of the computational domain.

In the time-marching calculations of the multiple solutions of SCF, the final solution depends on the initial conditions (initial flowfield, transient effects like temporary counter-rotation of the outer sphere and the perturbation used). In this work, we use a perturbation velocity similar to that used to trigger traveling waves in circular Couette flow (Schroeder and Keller 1990);

$$\begin{aligned} v_r' &= -4\varepsilon_1 \frac{(r - R_1)(r - R_2)}{(R_2 - R_1)^2} \cos \left[\pi \left(1 - \frac{R_m \left(\frac{\pi}{2} - \theta \right)}{(R_1 - R_2)} - \varepsilon_2 \sin(m_a \phi) \right) \right], \\ v_\theta' &= \varepsilon_1 \sin \left[\frac{\pi (r - R_1)(r - R_m)(r - R_2)}{2(R_2 - R_1)^3} \right] \sin \left[\pi \left(1 - \frac{R_m \left(\frac{\pi}{2} - \theta \right)}{(R_1 - R_2)} - \varepsilon_2 \sin(m_a \phi) \right) \right] \frac{1}{\beta}, \end{aligned} \quad (1)$$

where $R_m = 0.5(R_1 + R_2)$, $\varepsilon_1 = 10^{-4}$ is the perturbation amplitude for velocity and $\varepsilon_2 = 0.4$ is the perturbation amplitude for the azimuthal variation. In Yuan (2012), different values of the azimuthal wave number m_a have used to initialize different numbers of spiral waves at the same Reynolds number for $\beta = 0.18$. But for present wide-gap cases, the formation of spiral

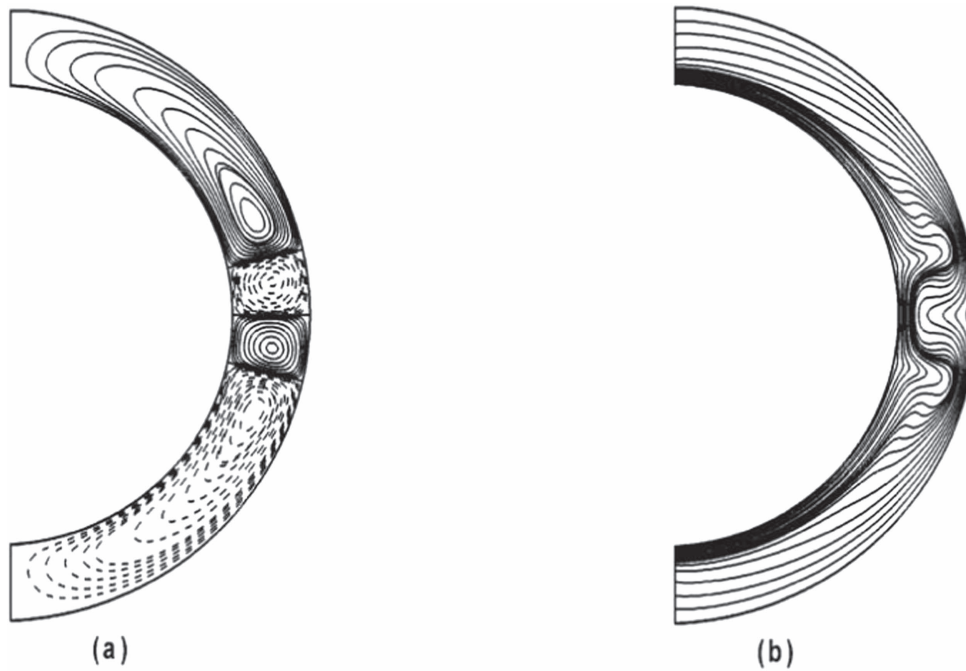


Figure 1. Steady 1-vortex flow for $\beta = 0.33$ at $\text{Re} = 700$: (a) streamlines; (b) angular velocity $u_\phi/r \sin(\theta)$.

waves are independent of the value of m_a used. So we have fixed the wave number $m_a = 6$ in all cases. We have added the perturbation (1) to the numerical solution at each time step, and this was done for a duration of the non-dimensional viscous diffusion time across the gap which is $t_d = \beta^2 \text{Re}$.

3. Results and discussion

We study two clearance ratios, $\beta = 0.33$ and $\beta = 0.50$ in the wide-gap regime defined by Nakabayashi *et al* (2002). The Reynolds number range studied is $450 \leq \text{Re} \leq 5000$ for $\beta = 0.33$, and $1250 \leq \text{Re} \leq 2500$ for $\beta = 0.50$. Computed results are compared with existing experimental (Egbers and Rath 1995, Liu *et al* 1996, Wulf *et al* 1999) and numerical results (Hollerbach 1998, Hollerbach *et al* 2006).

3.1. $\beta = 0.33$

For this clearance ratio, we cannot obtain the TG vortex flow directly from the Stokes flow. But numerical studies (Schrauf 1986, Hollerbach 1998, Loukopoulos and Karahalios 2004) showed that one can get TG vortices for $\beta \leq 0.4963$ by means of special conditions, e.g., Hollerbach (1998) obtained the TG vortex for $\beta = 0.336$ by starting with the stable Taylor vortex flow for $\beta = 0.154$, then gradually increasing β up to the desired value. In our study, we first obtained the steady toroidal 1-vortex flow for $\beta = 0.33$ at $\text{Re} = 700$ by using the 1-vortex flow computed for $\beta = 0.18$ at $\text{Re} = 700$ as the initial condition. Figure 1 shows the meridional streamlines and angular velocity for $\beta = 0.33$ at $\text{Re} = 700$. By scanning the

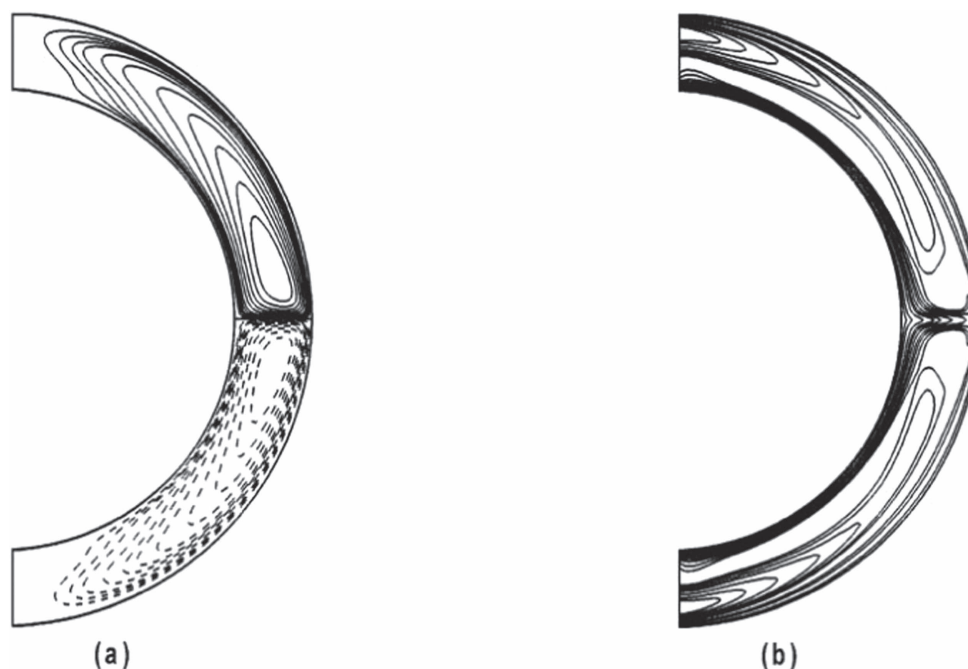


Figure 2. Azimuthally averaged section contours for the $m = 5$ spiral waves for $\beta = 0.33$, $\text{Re} = 2900$: (a) meridional streamlines; (b) angular velocity $u_\phi/(r \sin \theta)$.

Reynolds number range first with $\Delta \text{Re} = 100$ then with $\Delta \text{Re} = 10$ to determine the critical Reynolds number, the 1-vortex flow is found to exist for $\text{Re} \in [450, 2050]$. The flow then evolves from the 1-vortex flow to the basic 0-vortex flow when $\text{Re} > 2050$, and this trend is consistent with the experimental and numerical results (Liu *et al* 1996, Hollerbach 1998).

We explore spiral instabilities by increasing the Reynolds number starting from the 0-vortex flow at $\text{Re} = 2600$. For the purpose of comparison, we first describe previous experimental visualization results. According to the experiment of Egbers and Rath (1995), secondary waves of an azimuthal wavenumber $m = 6, 5$ and 4 occur in turn and then the flow becomes turbulent with increasing Reynolds number. However, the experiment of Wulf *et al* (1999) first observed a corotating spiral vortex with its center in the pole, then at a higher Reynolds number the spiral vortex turns into a ring vortex that originates periodically in the middle latitude zone, travels to the polar region and vanishes at the pole. Increasing Reynolds number further, the ring vortex disintegrates into spiral waves of wavenumber $m = 6$ in the middle latitude zone, then three of the six spiral waves become weak and finally the flow becomes turbulent.

By using an increment of $\Delta \text{Re} = 10$ and starting from the 0-vortex flow at $\text{Re} = 2600$, we obtained an approximate critical Reynolds number $\text{Re}_{c1} = 2900$ for the occurrence of spiral waves with wavenumber $m = 6$. This value is larger than $\text{Re}_{c1} = 2628$ for the occurrence of spiral waves with wavenumber $m = 6$ in Egbers and Rath (1995), and much larger than $\text{Re}_{c1} = 2395$ for the occurrence of a spiral vortex centering at the pole in Wulf *et al* (1999). Figures 2(a) and (b) show the computed contours of azimuthally averaged meridional streamlines and angular velocity $u_\phi/(r \sin \theta)$ at $\text{Re}_{c1} = 2900$. It can be seen from

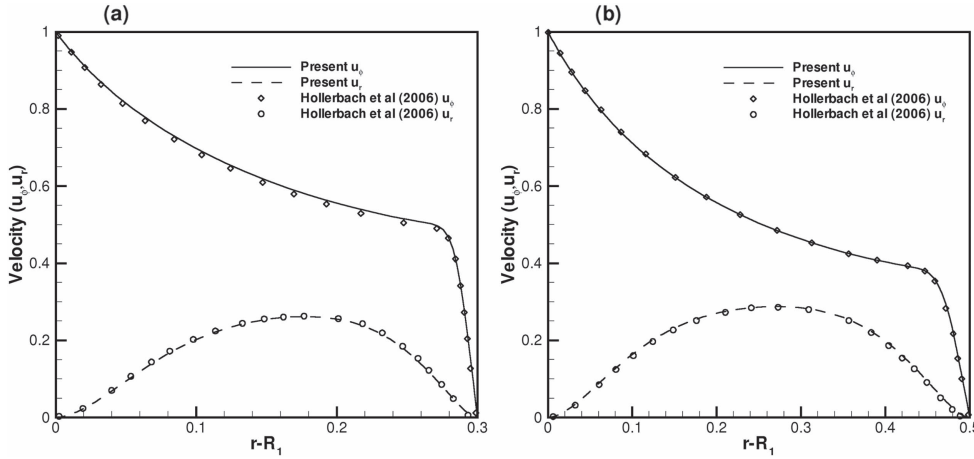


Figure 3. Comparison of the present azimuthally averaged u_ϕ (solid) and u_r (dashed) as a function of $r - R_1$ for (a) the $m = 6$ spiral wave flow at $Re = 2900$, $\beta = 0.30$, (b) the $m = 5$ spiral wave flow at $Re = 1280$, $\beta = 0.50$ with the numerical results of Hollerbach *et al* (2006) u_ϕ (diamonds) and u_r (circles) for the $m = 6$ spiral wave flow at $Re = 3310$, $\beta = 0.30$, and the $m = 5$ spiral wave flow at $Re = 1245$, $\beta = 0.50$, respectively.

figure 2(b) that the meridional flow has two different flow structures, a strong equatorial jet and a strong boundary layer adjacent to the inner sphere.

To verify the correctness of our code, figure 3 shows a comparison of the distributions of velocity components u_ϕ (solid) and u_r (dashed) as a function of the radial distance relative to the inner sphere (radius) in the equatorial plane with the numerical results in Hollerbach *et al* (2006) for $\beta = 0.30$ and 0.50 . The comparison shows that our results agree well with those of Hollerbach *et al* (2006). It can be seen that the rotational velocity u_ϕ is much larger than the radial velocity u_r .

Figure 4 shows the north pole view of the colored contours for the azimuthal vorticity at four typical Reynolds numbers. Starting from $Re_{c1} = 2900$, spiral waves of wavenumber $m = 6$ appear first. These spiral waves appear in the middle latitudes and extend towards the polar region up to $Re \approx 2990$. By increasing the Reynolds number to $Re_{c2} = 3000$, we obtained spiral waves of wavenumber $m = 5$ and these five spiral waves remain stable up to $Re \approx 3900$. When we further increasing the Reynolds number to $Re_{c3} = 4000$, the spiral wavenumber is reduced to $m = 4$ and these four spiral waves exist up to $Re_{c4} = 4500$. Like spiral waves with wavenumber $m = 6$, the spiral waves of wavenumber $m = 5$ and 4 also appear periodically in the middle latitudes and extend towards the polar region. When $Re > Re_{c4}$, the spiral structures start to break up and we obtain aperiodic coherent structures which cause the flow to become turbulent at $Re = 5000$. Hence we can say that our scenario is $m = 6 \rightarrow 5 \rightarrow 4 \rightarrow$ turbulence, as was found by Egbers and Rath (1995).

Figure 5 shows the radial velocity contours u_r in the unwrapped middle spherical surface $r = 1 + 0.5\beta$, $0 \leq \theta \leq \pi$, $0 \leq \phi \leq 2\pi$. Although we have imposed the perturbation (1) with a fixed $m_a = 6$ for a duration of $\delta t = \mathcal{O}(\beta^2 Re)$ in the computation, the final wavenumber $m = 6, 5$ or 4 of the spiral waves only depends on the Reynolds number. The outflow boundary at the equator is wavy in the ϕ direction in the case of $Re = 5000$ due to the strong secondary flow convection of the spiral structures toward the equatorial region.

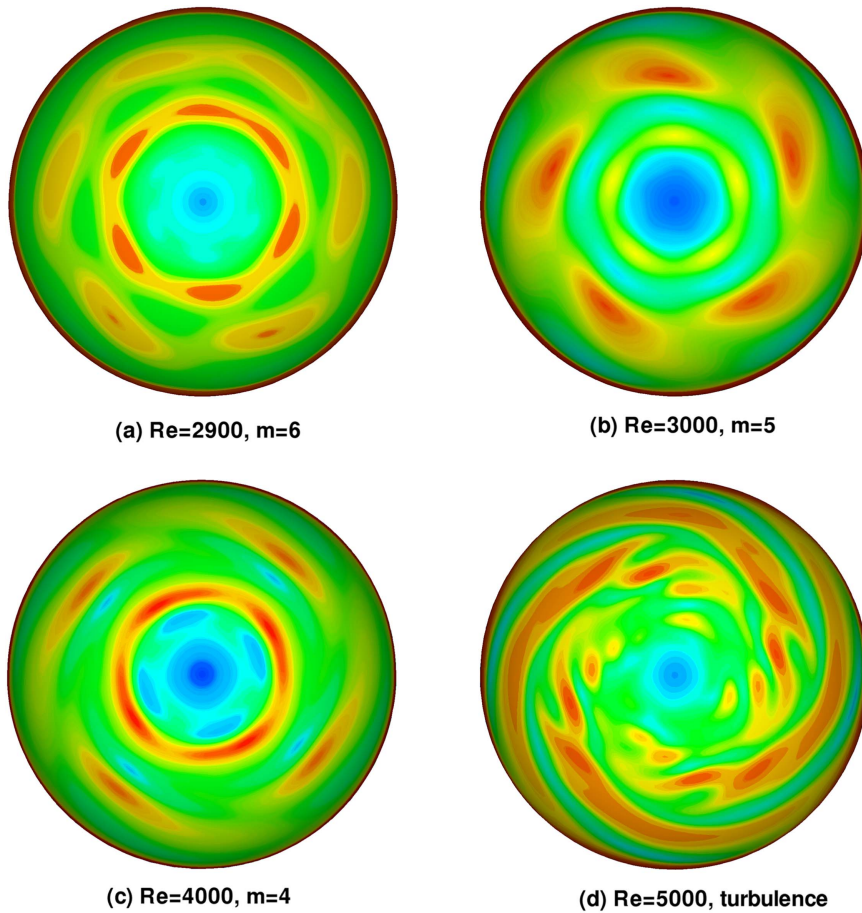


Figure 4. North pole view of the colored contours of the azimuthal vorticity component ω_ϕ of spiral waves for $\beta = 0.33$ at four different Re. The inner sphere rotates counterclockwise.

Figure 6 shows the time history of u_θ at a point in the flowfield for $m = 6, 5, 4$ and turbulent flows. From the corresponding data, we have calculated the non-dimensional rotational frequencies of the spiral waves according to $\frac{f_{\text{rot}}}{f} = \frac{2\pi}{T_{\text{rot}}}$ as in Yuan (2012), where f is the dimensional rotational frequency of the inner sphere and T_{rot} is the non-dimensional rotational period of the spiral waves as a whole. We measured the rotational frequency $\frac{f_{\text{rot}}}{f} = 1.70$ for $m = 6$ at $\text{Re} = 2900$, $\frac{f_{\text{rot}}}{f} = 1.60$ for $m = 5$ at $\text{Re} = 3000$ and $\frac{f_{\text{rot}}}{f} = 1.06$ for $m = 4$ at $\text{Re} = 4000$ respectively. These numbers are roughly close to 1.79, 1.56 and 1.13 for $m = 6$ at $\text{Re} = 2680$, $m = 5$ at $\text{Re} = 2855$ and $m = 4$ at $\text{Re} = 3142$ respectively as given in figure 10 of Egbers and Rath (1995).

Finally, we show the evolution of the wavenumber with increasing or decreasing Reynolds number in figure 7(a) for $\beta = 0.33$. The evolution path with increasing Reynolds number is marked with the rightward arrows while that with decreasing Reynolds number is marked with the leftward arrows. Hysteresis, i.e. the difference between the two paths, was observed in the experiments of Egbers and Rath (1995). To obtain the decreasing path, first we have used the numerical solution of spiral waves of wavenumber $m = 5$ at $\text{Re}_{c2} = 3000$

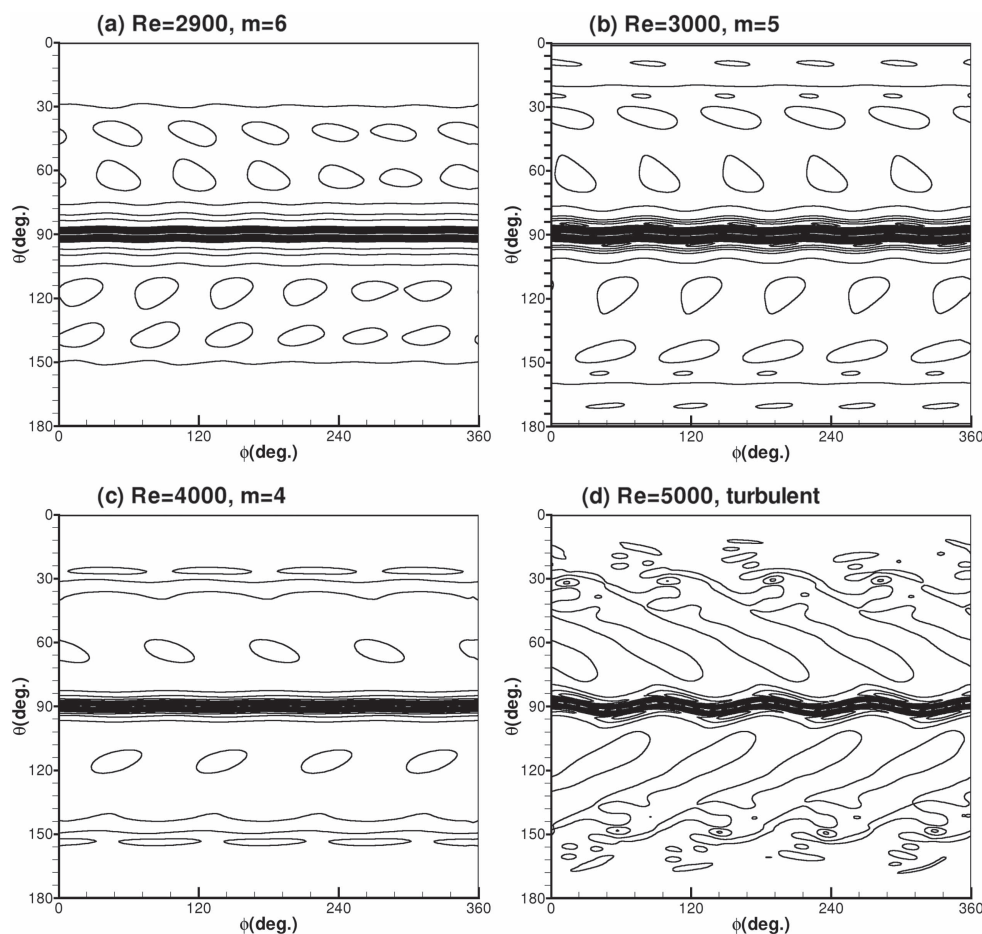


Figure 5. Contours of the radial velocity u_r , at different Re on the middle spherical surface $r = 1 + 0.5\beta$, $0 \leq \theta \leq \pi$, $0 \leq \phi \leq 2\pi$ for $\beta = 0.33$.

as an initial condition and reduced the Reynolds number with $\Delta Re = 10$. We have found that with decreasing Reynolds number, the spiral waves of wavenumber $m = 5$ remain stable down to $Re \approx 2910$. With further decreasing Reynolds number, we have successfully recovered the preceding solution with $m = 6$ spiral waves at $Re = 2900$. Thus we have obtained a small hysteresis loop. Next we have used the solution of spiral waves of wavenumber $m = 4$ at $Re_{c3} = 4000$ as an initial condition and reduced the Reynolds number with $\Delta Re = 10$. We have found that the spiral waves of wavenumber $m = 4$ remain stable down to $Re \approx 3100$. Further decreasing the Reynolds number we have recovered the preceding solution with $m = 5$ spiral waves at $Re = 3000$. This forms another larger hysteresis loop. Due to the limited numerical resolution, the thresholds in figure 7 are approximate. In addition, a bifurcation analysis would explain the structure behind these hysteresis loops.

3.2. $\beta = 0.50$

For this wide-gap case, the first instability appears in the form of rotating spiral waves with wavenumber $m = 5$, and the present transition scenario with increasing Reynolds

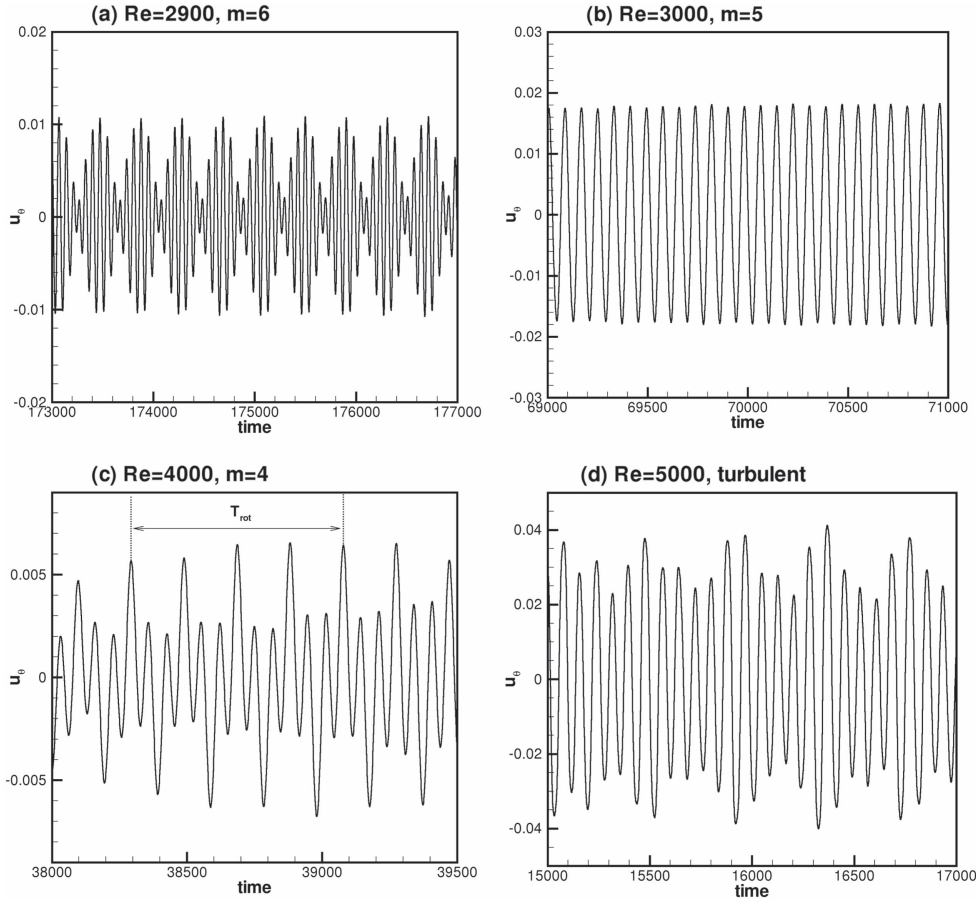


Figure 6. Time history of the meridional velocity component u_θ at a point $(r, \theta, \phi) = (1 + \beta/2, \pi/2, 0)$ for $\beta = 0.33$. The rotational period T_{rot} of the spiral waves is counted between every four peaks for the $m = 4$ case as shown in frame (c).

number is $m = 5 \rightarrow 4 \rightarrow 5 \rightarrow 4 \rightarrow 3 \rightarrow$ turbulence, which partially follows that of $m = 5 \rightarrow 4 \rightarrow 3 \rightarrow$ turbulence as in Egbers and Rath (1995) and partially follows that of $m = 5 \rightarrow 4 \rightarrow 3 \rightarrow 5 \rightarrow 4 \rightarrow$ turbulence as in Wulf *et al* (1999). Recall that Egbers and Rath (1995) obtained secondary waves of wavenumber $m = 5$ at $Re_{c1} = 1244$, and by increasing the Reynolds number, the wavenumber decreases to 4 at $Re = 1583$ and to 3 at $Re = 1810$ and then the flow becomes turbulent at higher Reynolds numbers. On the other hand, Wulf *et al* (1999) obtained $m = 5$ at $Re_{c1} = 1190$, then $m = 4$ at $Re_{c2} = 1395$ and then $m = 3$ at $Re_{c3} = 1565$. However, by further increasing the Reynolds number, they obtained traveling spiral waves of wavenumber $m = 5$ at $Re_{c4} = 1710$ and aperiodic spiral waves of wavenumber $m = 4$ at $Re_{c5} = 2080$ and then the flow becomes chaotic for $Re \geq Re_{c6} \approx 2380$. In previous numerical studies, Araki *et al* (1997) and Hollerbach *et al* (2006) obtained spiral waves of wavenumber $m = 5$ at different critical Reynolds numbers $Re_c = 1245$ and 1431 respectively. Unlike Egbers and Rath (1995) and Wulf *et al* (1999), they did not show the evolution of the flow states with increasing Reynolds number.

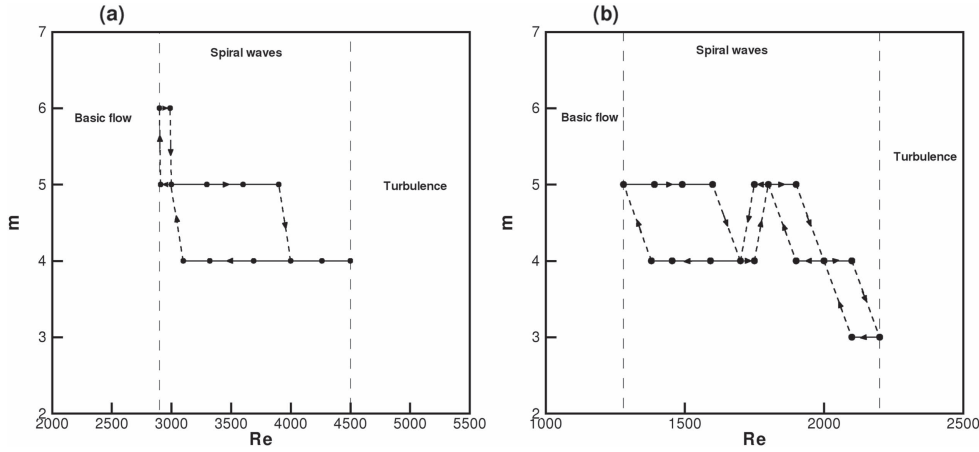


Figure 7. Transition path and hysteresis effect for the flow of spiral waves of different spiral wavenumber m with increasing or decreasing Reynolds number, (a) $\beta = 0.33$, (b) $\beta = 0.50$.

In the present study, we show the transition scenario with increasing Reynolds number. First to verify the accuracy of the present code, figure 3(b) shows comparison of the present velocity u_ϕ and velocity u_r (averaged in the ϕ direction) as a function of radius in the equatorial plane at $Re_{c1} = 1280$ for spiral waves of wavenumber $m = 5$ with the numerical results of Hollerbach *et al* (2006) at $Re_c = 1245$, and the agreement is good.

We have found the critical Reynolds number to be $Re_{c1} = 1280$ where the spiral waves of wavenumber $m = 5$ occur first and rotate in the same direction as the inner sphere. With increasing Reynolds number, flow states with different wave numbers and shapes appear as shown in figure 8. We note that the $m = 5$ spiral waves are succeeded by the $m = 4$ spiral waves at $Re_{c2} = 1700$ as shown in figure 8(b). When we further increase the Reynolds number, the flow evolves into a ring wave encircling the pole and the $m = 5$ traveling spiral waves in the low to medium latitude zones at $Re_{c3} = 1800$ as shown in figure 8(c). From the time snapshots (not shown here), we confirmed the observation (Wulf *et al* 1999) that the traveling spiral waves originate between the middle latitudes and the equatorial region and travel towards the polar region. As the Reynolds number is increased to $Re_{c4} = 2000$, the wavenumber of the spiral waves and ring waves reduces to $m = 4$ as shown in figure 8(d). By increasing the Reynolds number further to $Re_{c5} = 2200$, we obtained two separate $m = 3$ spiral waves that travel in the same direction as the rotation of the inner sphere and are separated synchronously with one set of spiral waves being near the polar region as show in figure 8(e). This figure looks like figure 9(c) of Wulf *et al* (1999). Finally at $Re = 2500$, the flow becomes turbulent and we get some instantaneous irregular structures as shown in figure 8(f). The present transition scenario is $m = 5 \rightarrow 4 \rightarrow 5 \rightarrow 4 \rightarrow 3 \rightarrow$ turbulence, which only partially resembles those in Egbers and Rath (1995) and Wulf *et al* (1999).

The evolution of these flow states in terms of the spiral wavenumber with increasing Reynolds number (rightward arrows) and decreasing Reynolds number (leftward arrows) are shown in figure 7(b). As we did for $\beta = 0.33$, we have used the solutions at critical Reynolds numbers obtained in the forward path as the initial conditions. We then reduced the Reynolds number until we recovered the preceding spiral wavy flow at a lower Reynolds number. The

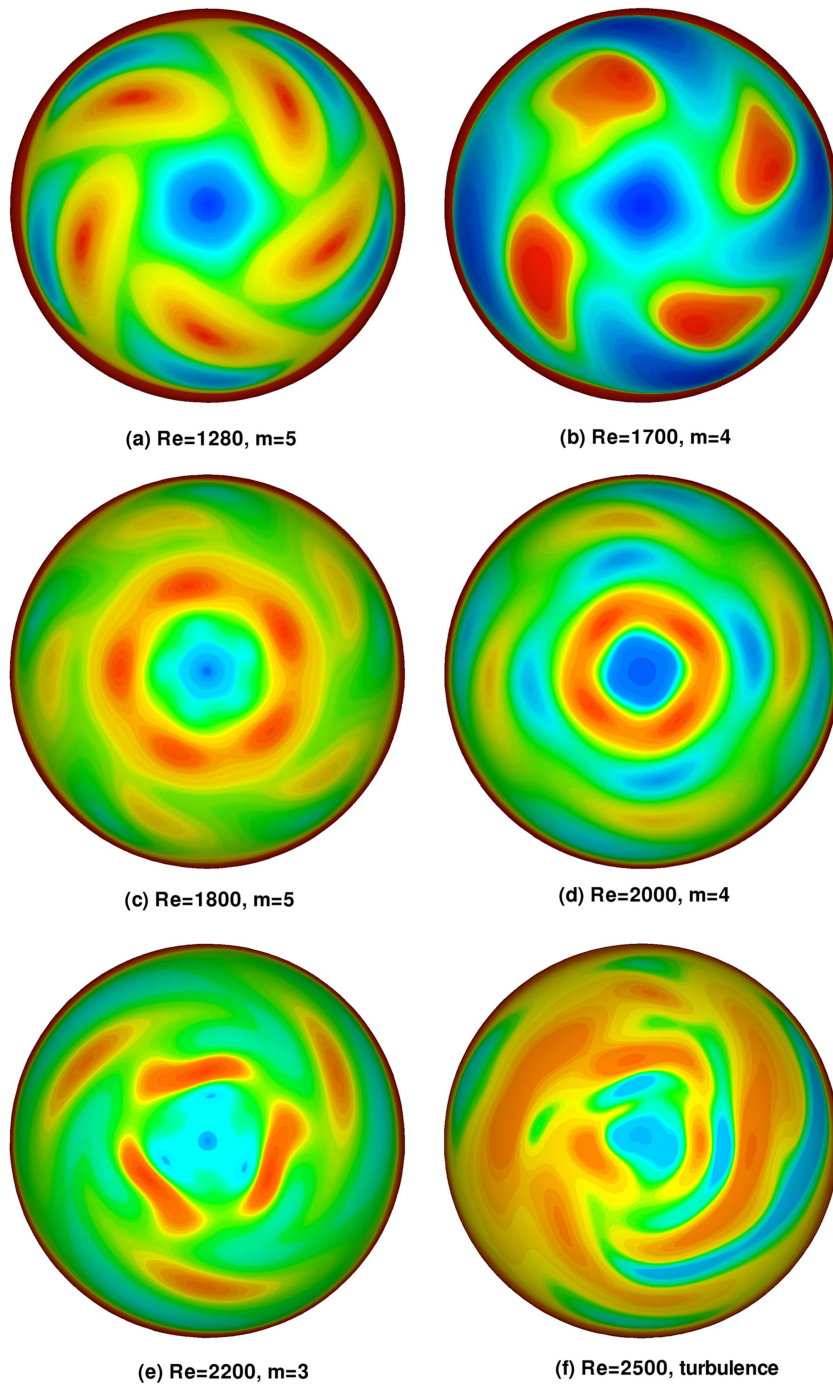


Figure 8. North pole view of flooded contours of the azimuthal vorticity component ω_ϕ of the spiral wave flows for $\beta = 0.50$, (a) $m = 5$ spiral waves; (b) $m = 4$ spiral waves; (c) five traveling spiral waves; (d) four aperiodic spiral waves; (e) two sets of three spiral waves; (f) turbulence. The inner sphere rotates counterclockwise. Reproduced from Araki *et al* (1997), with the permission of AIP Publishing. <http://doi.org/10.1063/1.869177>.

differences between forward and backward paths form hysteresis loops, which can be observed in figure 7(b).

To see the flow structures more clearly, figure 9 shows contours of the radial velocity u_r in the unwrapped spherical surface $r = 1 + 0.7\beta$, $0 \leq \theta \leq \pi$, $0 \leq \phi \leq 2\pi$. As in figure 5, the outflow boundary at the equator is wavy in the ϕ direction due to the influence of the spiral waves.

Figure 10 shows the time history of the meridional velocity component u_θ at an interior point $(r, \theta, \phi) = (1 + 0.7\beta, \pi/2, 0)$. As we did in figure 6, we have computed the rotational frequencies of the spiral waves. The non-dimensional rotational frequencies are $\frac{f_{rot}}{f} = 1.37$, 1.06 and 0.75 for $m = 5$ at $Re = 1280$, $m = 4$ at 1700, and $m = 3$ at 2200 respectively. These values are in fair agreement with 1.32, 1.05 and 0.75 at $Re = 1190$, 1395 and 1565 respectively of Wulf *et al* (1999), and close to 1.36, 0.97 for $m = 5, 4$ at $Re = 1700, 1810$ extracted from figure 10 in Egbers and Rath (1995).

4. Conclusions

We have numerically investigated the wide-gap SCF with a rotating inner sphere. Two clearance ratios $\beta = 0.33$ and $\beta = 0.50$ have been studied for a wide range of Reynolds numbers covering laminar basic flows, spiral instabilities, and turbulent flows.

We have obtained the 1-vortex flow for $\beta = 0.33$ in the range of $Re \in [450, 2050]$ by using a special initial condition. This confirmed previous numerical (Schrauf 1986, Hollerbach 1998, Loukopoulos and Karahalios 2004) and experimental results (Liu *et al* 1996, Junk and Egbers 2000) that TG vortices can exist for wide-gap cases. In addition, the computed velocity distributions along the radius at the equator for $\beta = 0.30$ and 0.50 are in good agreement with available numerical results. Subsequently, we simulated the transition scenarios of flow states with increasing Reynolds number.

For $\beta = 0.33$, we obtained spiral waves of wavenumber $m = 6$ at a critical Reynolds number $Re_c = 2900$ as compared to $Re_c = 2628$ in the experiment of Egbers and Rath (1995). When the Reynolds number is increased, the wavenumber of spiral waves decreases to 5 and 4 in turn and finally the flow becomes turbulent. Our scenario agrees with Egbers and Rath (1995), but disagrees with Wulf *et al* (1999) who obtained a rotating spiral vortex at the pole first at $Re_c = 2395$. The rotational frequencies of spiral waves with wavenumbers $m = 6, 5, 4$ are found to decrease with increasing Reynolds number, which agrees with the experimental results of Egbers and Rath (1995).

For $\beta = 0.50$, we obtained five spiral waves at a critical Reynolds number $Re_c = 1280$ very close to $Re_c = 1244$ of Egbers and Rath (1995). By increasing the Reynolds number we obtained periodic five and four spiral waves. Further increasing the Reynolds number, we obtained five spiral waves together with a ring wave near the pole, then four spiral waves with a ring wave, and then two separate sets of three spiral waves, and finally the flow becomes turbulent. Our scenario $m = 5 \rightarrow 4 \rightarrow 5 \rightarrow 4 \rightarrow 3 \rightarrow$ turbulence is the same as those of Egbers and Rath (1995) and Wulf *et al* (1999) only in the initial $5 \rightarrow 4$ stage.

We have managed to resolve the discrepancy between the two experimental scenarios (Egbers and Rath 1995, Wulf *et al* 1999). The hysteresis of the flow states depending on whether the Reynolds number is increased or decreased is also simulated. The rotational frequencies of different spiral wavenumbers are found in fair agreement with the experimental results (Egbers and Rath 1995, Wulf *et al* 1999).

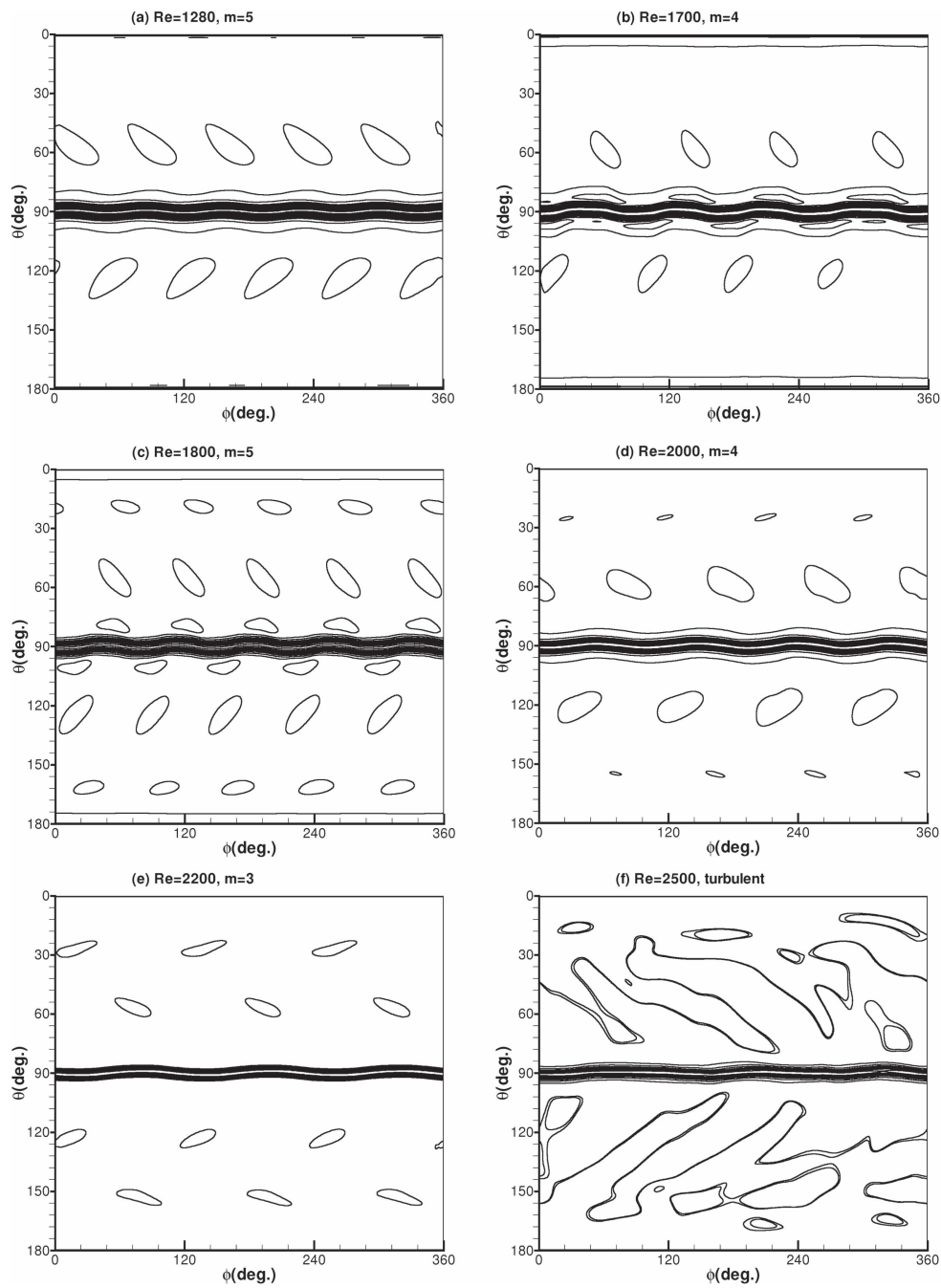


Figure 9. Contours of the radial velocity u_r for $\beta = 0.50$ at different Reynolds number on the unwrapped spherical surface $r = 1 + 0.7\beta$, $0 \leq \theta \leq \pi$, $0 \leq \phi \leq 2\pi$.

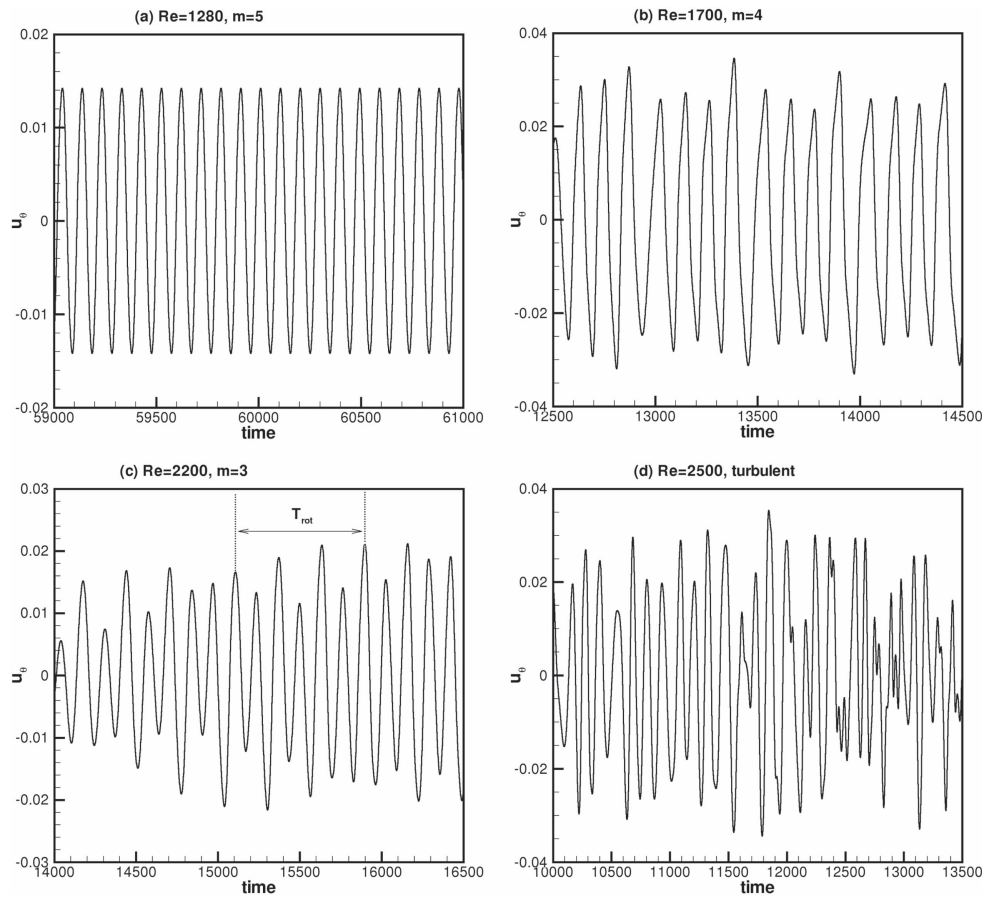


Figure 10. Time history of the meridional velocity component u_θ at a point $(r, \theta, \phi) = (1 + 0.7\beta, \frac{1}{2}\pi, 0)$ for $\beta = 0.50$. The rotational period T_{rot} of the spiral waves is counted between every three high peaks for $m = 3$ at $Re = 2200$ as shown in frame (c).

Acknowledgments

This work is supported by the Natural Science Foundation of China (11321061, 11261160486, and 91641107), State Key Program for Developing Basic Sciences (2010CB731505), and Fundamental Research of Civil Aircraft (MJ-F-2012-04). S Abbas thanks the support of CAS-TWAS President's Fellowship Program. We would also like to thank the anonymous referees for their useful comments and suggestions.

References

- Araki K, Mizushima J and Yanase S 1997 The nonaxisymmetric instability of the wide-gap spherical Couette flow *Phys. Fluids* **9** 1197–9
- Bartels F 1982 Taylor vortices between two-concentric rotating spheres *J. Fluid Mech.* **119** 1–65
- Belyaev Y N, Monakhov A A and Yavorskaya I M 1978 Stability of spherical Couette flow in thick layers when the inner sphere revolves *Fluid Dyn.* **13** 162–8

- Belyaev Y N and Yavorskaya I M 1991 Problems of stability and the beginning of chaos in closed hydrodynamic flows *Proc. Steklov Inst.* **1** 123–33
- Bühler K and Zierep J 1987 Dynamical instabilities and transition to turbulence in spherical gap flows *Proc. of the 1st European Turbulence Conf. on Advances in Turbulence* ed G Comte-Bellot and J Mathieu (Berlin: Springer) pp 16–26
- Dumas G 1991 Study of spherical Couette flow via 3D spectral simulations: large and narrow gap flows and their transitions *PhD Thesis* California Institute of Technology
- Dumas G and Leonard A 1994 A divergence-free spectral expansions method for three-dimensional flows in spherical-gap geometries *J. Comput. Phys.* **111** 205–19
- Egbers C and Rath H J 1995 The existence of Taylor vortices and wide-gap instabilities in spherical Couette flow *Acta Mech.* **111** 125–40
- Hollerbach R 1998 Time-dependent Taylor vortices in wide-gap spherical Couette flow *Phys. Rev. Lett.* **81** 31–2
- Hollerbach R 2000 A spectral solution of the magneto-convection equations in spherical geometry *Int. J. Numer. Methods Fluids* **32** 773–97
- Hollerbach R, Junk M and Egbers C 2006 Non-axisymmetric instabilities in basic state spherical Couette flow *Fluid Dyn. Res.* **38** 257–73
- Jiang G S and Wu C C 1999 A High-order WENO finite difference scheme for the equations of ideal magnetohydrodynamics *J. Comput. Phys.* **150** 561–94
- Junk M and Egbers C 2000 Isothermal spherical Couette flow *Physics of Rotating Fluids (Lecture Notes in Physics* vol 549) pp 215–35
- Liu M, Blohm C, Egber C, Wulf P and Rath H J 1996 Taylor vortices in wide spherical shell *Phy. Rev. Lett.* **77** 286
- Loukopoulos C and Karahalios T 2004 Taylor vortices in annular spherical flow at large aspect ratios *Phys. Fluids* **16** 27–08
- Marcus P and Tuckerman L 1987a Simulation of flow between two concentric rotating spheres: I. Steady states *J. Fluid Mech.* **185** 1–30
- Marcus P and Tuckerman L 1987b Simulations of flow between two concentric rotating spheres: II. Transitions *J. Fluid Mech.* **185** 31–65
- Munson B R and Menguturk M 1975 Viscous incompressible flow between concentric rotating spheres: Linear stability and experiments *J. Fluid Mech.* **69** 705–19
- Nakabayashi K 1983 Transition of Taylor–Görtler vortex flow in spherical Couette flow *J. Fluid Mech.* **132** 209–30
- Nakabayashi K and Tsuchida Y 1995 Flow-history effect on higher modes in the spherical Couette flow *J. Fluid Mech.* **295** 43–60
- Nakabayashi K, Tsuchida Y and Zheng Z 2002 Characteristics of disturbances in the laminar-turbulent transition of spherical Couette flow: I. Spiral Taylor–Görtler vortices and traveling waves for narrow gaps *Phys. Fluids* **14** 3963–72
- Rogers S and Kwak D 1990 Upwind differencing scheme for the time-accurate incompressible Navier–Stokes equations *AIAA J.* **28** 253–62
- Sawatzki O and Zierep J 1970 Das Stromfeld im Spalt zwischen zwei konzentrischen Kugelflächen, von denen die innere rotiert *Acta Mech.* **9** 13–35
- Schrauf G 1986 The first instability in spherical Couette flow *J. Fluid Mech.* **166** 287–303
- Schroeder W and Keller H 1990 Wavy Taylor-vortex flows via multigrid-continuation methods *J. Comput. Phys.* **91** 197–227
- Sha W and Nakabayashi K 2001 On the structure and formation of spiral Taylor–Görtler vortices in spherical Couette flow *J. Fluid Mech.* **431** 323–45
- Wimmer M 1976 Experiments on a viscous fluid flow between concentric rotating spheres *J. Fluid Mech.* **78** 317–35
- Wimmer M 1988 Viscous flow and instabilities near rotating bodies *Prog. Aerosp. Sci.* **25** 43–103
- Wulf P, Egbers C and Rath H J 1999 Routes to chaos in wide-gap spherical Couette flow *Phys. Fluids* **11** 1359–72
- Yang J Y, Yang S C, Chen Y N and Hsu C A 1998 Implicit weighted ENO schemes for three-dimensional incompressible Navier–Stokes equations *J. Comput. Phys.* **146** 464–87
- Yavorskaya I, Belyaev Y, Monakhov A, Astaf N, Scherbakov S and Vvedenskaya N 1980 Stability, nonuniqueness and transition to turbulence in the flow between two rotating spheres *Report No. 595* Space Research Institute of the Academy of Science, USSR

- Yuan L 2002 Comparison of implicit multigrid schemes for three-dimensional incompressible flows *Comput. Phys.* **77** 134–55
- Yuan L 2004 Numerical study of multiple periodic flow states in spherical Taylor–Couette flow *Sci. China A* **47** 81–91
- Yuan L 2012 Numerical investigation of wavy and spiral Taylor–Görtler vortices in medium spherical gaps *Phys. Fluids* **24** 124104
- Yuan L, Fu D X and Ma Y W 1996 Numerical study of bifurcation solutions of spherical Taylor–Couette flow *Sci. China A* **39** 187–96
- Zikanov O 1996 Symmetry-breaking bifurcations in spherical Couette flow *J. Fluid Mech.* **310** 293–324